JCI The Journal of Clinical Investigation

Yersinia pseudotuberculosis disrupts intestinal barrier integrity through hematopoietic TLR-2 signaling

Camille Jung, … , Jean-Pierre Hugot, Frederick Barreau

J Clin Invest. 2012;122(6):2239-2251. https://doi.org/10.1172/JCI58147.

Research Article **Gastroenterology**

Intestinal barrier function requires intricate cooperation between intestinal epithelial cells and immune cells. Enteropathogens are able to invade the intestinal lymphoid tissue known as Peyer's patches (PPs) and disrupt the integrity of the intestinal barrier. However, the underlying molecular mechanisms of this process are poorly understood. In mice infected with *Yersinia pseudotuberculosis*, we found that PP barrier dysfunction is dependent on the *Yersinia* virulence plasmid and the expression of TLR-2 by hematopoietic cells, but not by intestinal epithelial cells. Upon TLR-2 stimulation, *Y. pseudotuberculosis*–infected monocytes activated caspase-1 and produced IL-1β. In turn, IL-1β increased NF-κB and myosin light chain kinase activation in intestinal epithelial cells, thus disrupting the intestinal barrier by opening the tight junctions. Therefore, *Y. pseudotuberculosis* subverts intestinal barrier function by altering the interplay between immune and epithelial cells during infection.

Yersinia pseudotuberculosis disrupts intestinal barrier integrity through hematopoietic TLR-2 signaling

Camille Jung,[1,2,3] Ulrich Meinzer,[1,2] Nicolas Montcuquet,[4,5] Elodie Thachil,[1,2] Danielle Château,[6] Raphaële Thiébaut,[1,2] Maryline Roy,[1,2] Ziad Alnabhani,[1,2] Dominique Berrebi,[1,2,3] Monique Dussaillant,[1,2] Eric Pedruzzi,[1,7] Sophie Thenet,[6,8,9] Nadine Cerf-Bensussan,[4,5] Jean-Pierre Hugot,[1,2,3] and Frederick Barreau[1,2]

[1]Université Paris-Diderot, UMR843, Paris, France. [2]INSERM, UMR843, Paris, France. [3]Assistance Publique Hôpitaux de Paris, Hôpital Robert Debré, Paris, France. [4]INSERM U989, Paris, France. [5]Université Paris Descartes, Faculté de Médecine René Descartes, Paris, France. [6]INSERM, U872, Paris, France. [7]INSERM, U773, Centre de Recherche Bichat-Beaujon CRB3, Paris, France. [8]Université Paris Descartes-Paris 5, UMR S 872, Paris, France. [9]Ecole Pratique des Hautes Etudes, Paris, France.

Intestinal barrier function requires intricate cooperation between intestinal epithelial cells and immune cells. Enteropathogens are able to invade the intestinal lymphoid tissue known as Peyer's patches (PPs) and disrupt the integrity of the intestinal barrier. However, the underlying molecular mechanisms of this process are poorly understood. In mice infected with *Yersinia pseudotuberculosis*, we found that PP barrier dysfunction is dependent on the *Yersinia* virulence plasmid and the expression of TLR-2 by hematopoietic cells, but not by intestinal epithelial cells. Upon TLR-2 stimulation, *Y. pseudotuberculosis*–infected monocytes activated caspase-1 and produced IL-1β. In turn, IL-1β increased NF-κB and myosin light chain kinase activation in intestinal epithelial cells, thus disrupting the intestinal barrier by opening the tight junctions. Therefore, *Y. pseudotuberculosis* subverts intestinal barrier function by altering the interplay between immune and epithelial cells during infection.

Introduction

The intestinal mucosa is the largest interface between the host and its environment. It forms a barrier that limits the entrance of the luminal commensal bacteria and pathogens (1). This barrier is not fully impermeable, but allows the passage of small amounts of molecules from the intestinal lumen to the internal milieu through 2 mechanisms: paracellular diffusion and transcellular transport. The paracellular permeability allows passage of small molecules and is determined by the pore size of tight junctions (TJs). The mechanisms underlying the structural and functional modifications of TJs include endocytosis of junctional proteins, epithelial apoptosis, and activation of the myosin light chain kinase (MLCK). MLCK activation opens the TJs (2), whereas MLCK inhibition prevents the increase in paracellular permeability (3).

Intestinal barrier function results from cooperation between epithelial and immune cells. DCs may sample bacteria directly from the intestinal lumen by extending their dendrites between intestinal epithelial cells (IECs). However, the transcellular transport of large particles, including microbes and antigens, has traditionally been ascribed to M cells overlying Peyer's patches (PPs). M cells are particularly involved in the transcytosis of bacteria, owing to their structural and molecular features, including expression of receptors such as TLRs at their apical surfaces. M cells bind, internalize, and transport macromolecules and release them in the underlying vicinity of immune cells present in the PPs. Thus, PPs constantly sample macromolecules from the intestinal lumen into the inductive sites of the intestinal immune system (4) and induce the homeostatic tolerogenic immune response to dietary antigens.

The proximity of epithelial and immune cells in PPs allows a permanent interaction between them. Thus, increased intestinal permeability causes activation of immune cells and contributes to the development of local and systemic inflammation (5). In turn, immune cells are involved in the disturbance of intestinal barrier function (6). When activated, they may secrete cytokines, chemokines, and other molecules, some of which have previously been shown to influence paracellular and/or transcellular permeabilities (7–9). IL-1β increases paracellular permeability by upregulating the expression and activity of epithelial MLCK (9, 10). However, the mechanisms underlying the interactions between epithelial cells and immune cells in PPs, as well as the resulting regulation of paracellular and transcellular permeabilities, are poorly understood.

In order to decide between immune tolerance of the commensal gut flora and the inflammatory response toward detrimental pathogens, the intestinal mucosa expresses a large number of receptors. TLRs are well-known ligands for microbe-associated molecular patterns and are widely expressed on various cell types within the gut mucosa. TLR-2 is expressed on IECs (11) as well as macrophages (12) and DCs (13). TLR-2 recognizes bacterial lipopeptides (14). Following activation by its ligands, TLR-2 activates the myeloid differentiation factor–88 adaptor (MYD88) (15). Mice deficient for *Tlr2* or *Myd88* display reduced expression of tissue-protective mediators and impaired intestinal homeostasis (15). In PPs, TLR-2 activation enhances transepithelial transport of microparticles (16).

Several enteropathogenic bacteria, including *Yersinia pseudotuberculosis* and *Yersinia enterocolitica* as well as *E. coli*, *Mycobacterium avium paratuberculosis*, *Listeria monocytogenes*, *Salmonella typhimurium*, and *Shi-*

Authorship note: Camille Jung and Ulrich Meinzer contributed equally to this work.
Conflict of interest: The authors have declared that no conflict of interest exists.
Citation for this article: *J Clin Invest.* 2012;122(6):2239–2251. doi:10.1172/JCI58147.

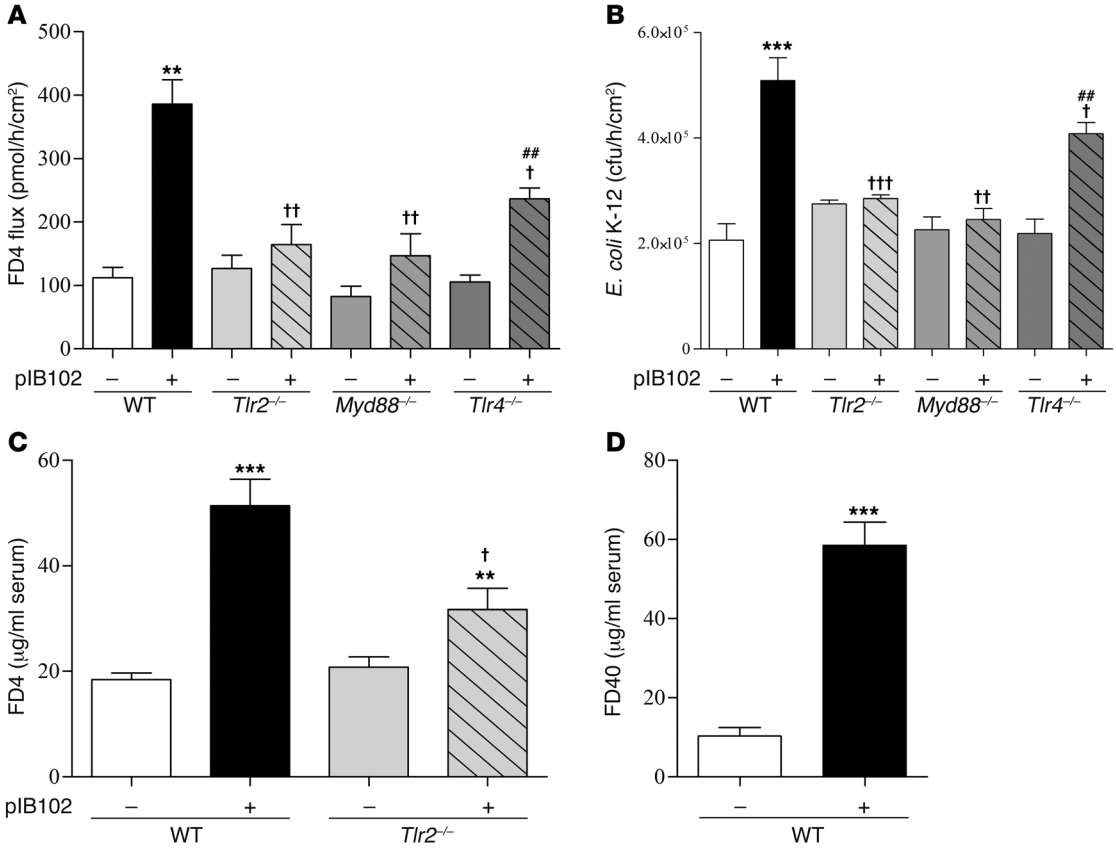

Figure 1

TLR2 is required for *Y. pseudotuberculosis* alteration of PP barrier function. (**A** and **B**) PPs from WT, *Tlr2*$^{-/-}$, *Tlr4*$^{-/-}$, and *Myd88*$^{-/-}$ mice were mounted in UCs and incubated with pIB102, and (**A**) paracellular permeability (i.e., FD4 flux) and (**B**) fluorescent *E. coli* K-12 translocation were monitored. (**C**) WT and *Tlr2*$^{-/-}$ mice were inoculated i.g. with pIB102, and paracellular permeability was investigated 5 days after infection. (**D**) WT mice were inoculated i.g. with pIB102, and transcellular permeability was investigated 5 days after infection. $n \geq 8$ per group; 3 independent experiments. $^{**}P < 0.01$, $^{***}P < 0.001$ versus uninfected WT; $^{\dagger}P < 0.05$, $^{\dagger\dagger}P < 0.01$, $^{\dagger\dagger\dagger}P < 0.001$ versus pIB102-infected WT; $^{\#\#}P < 0.01$ versus uninfected *Tlr4*$^{-/-}$.

gella flexneri, exploit the PP formations to invade their host (4). Invasion by *Y. pseudotuberculosis* depends on the bacterial surface protein invasin, which interacts with β1 integrins on the apical surface of M cells (17). Following their entry into PPs, the bacteria induce mucosal inflammation (18). In mice, oral inoculation with *Y. pseudotuberculosis* results in systemic bacterial translocation and subsequently in animal death (19, 20). TLR-2 plays a crucial role in initiating and regulating the host response to *Y. pseudotuberculosis* after oral infection (21); in contrast, it is dispensable for host defense after systemic infection (22). In humans, *Y. pseudotuberculosis* disturbs epithelial gut homeostasis and may induce ileitis (23–26). In patients with a history of *Y. pseudotuberculosis* infection, the intestinal barrier is altered for several months compared with healthy controls (24, 25). Here, we studied the mechanisms by which TLR-2 induces intestinal barrier dysfunction in the context of *Y. pseudotuberculosis* infection.

Results

The TLR-2 pathway contributes to Y. pseudotuberculosis–induced gut barrier dysfunction. To explore the effects of *Y. pseudotuberculosis* on paracellular and transcellular permeabilities, PPs were mounted in Ussing chambers (UCs) and exposed to *Y. pseudotuberculosis* strain YPIII(pIB102) (referred to herein as pIB102). Paracellular and transcellular routes were investigated by the flux of FITC-labeled 4-kDa dextran (FD4) and the translocation of killed fluorescent *E. coli*, respectively. Both parameters were greatly increased after pIB102 exposure (Figure 1, A and B). As *Y. pseudotuberculosis* is known to induce cell apoptosis, which modulates epithelial barrier function, we next determined the number of apoptotic cells induced by *Y. pseudotuberculosis*. 2 hours of incubation with pIB102 did not increase the number of caspase-3–positive apoptotic cells in PPs (Supplemental Figure 1 and Supplemental Methods; supplemental material available online with this article; doi:10.1172/JCI58147DS1). Next, we inoculated WT mice intragastrically (i.g.) with a single dose of pIB102. At day 5 after infection, infected mice received i.g. FD4 or FITC-labeled 40-kDa dextran (FD40); 5 hours later, increases of FD4 and FD40 serum concentrations were observed (Figure 1, C and D).

Because TLR-2 has previously been associated with *Yersinia* virulence (21), we tested its role in PP barrier dysfunction by reproducing the experiments in *Tlr2*$^{-/-}$ and *Myd88*$^{-/-}$ mice. In UCs, no differences in terms of PP permeability were observed at the basal level (Figure 1, A and B). In contrast, after pIB102 infection, we observed only a limited effect on the paracellular permeability and no effect on *E. coli* translocation in *Tlr2*$^{-/-}$ and *Myd88*$^{-/-}$ mice (Figure 1, A and B). Similarly, in vivo, FD4 levels were lower in the sera of *Tlr2*$^{-/-}$ mice (Figure 1C). Together, these findings suggested that TLR-2 contributes to *Y. pseudotuberculosis*–induced PP barrier dysfunction.

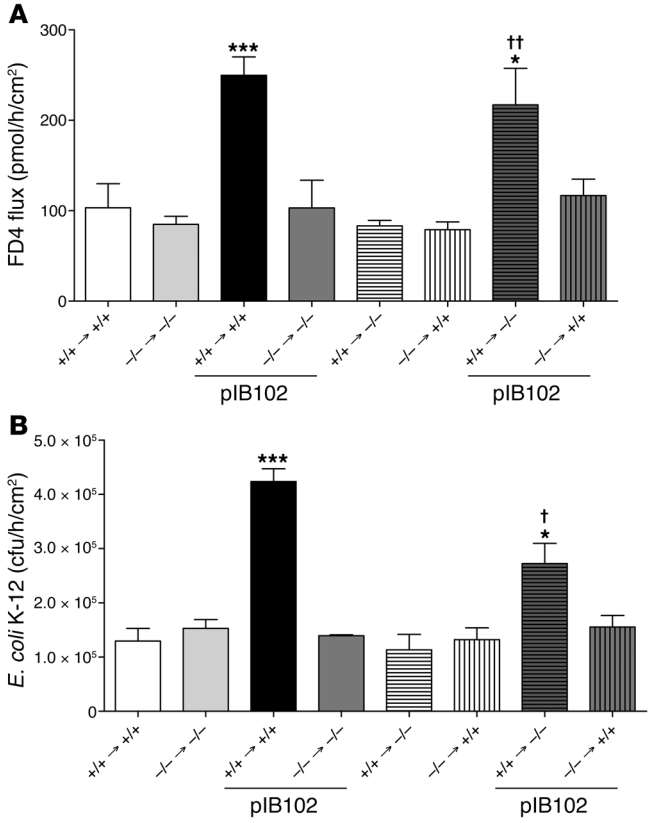

Figure 2
TLR2 from immune cells is required for *Y. pseudotuberculosis* disruption of PP barrier function. (**A** and **B**) PPs from chimeric mice, expressing TLR-2 (+/+) or not (–/–) in epithelial and immune cells, were mounted in UCs and incubated with pIB102, and (**A**) paracellular permeability and (**B**) fluorescent *E. coli* K-12 translocation were monitored. $n = 6$ per group; 2 independent experiments. $^{*}P < 0.05$, $^{***}P < 0.001$ versus uninfected +/+ → +/+; $^{\dagger}P < 0.05$, $^{\dagger\dagger}P < 0.01$ versus pIB102-infected –/– → +/+.

Since *Y. pseudotuberculosis* exhibits TLR-2 and TLR-4 agonists, and TLR-4 agonists are known to increase gut permeability (27), we also investigated the role of TLR-4. After pIB102 infection, a reduced (albeit significant) increase of paracellular permeability and *E. coli* translocation were observed in PPs from *Tlr4*$^{-/-}$ mice, whereas no differences were observed at the basal level (Figure 1, A and B). Taken together, these findings indicated that TLR-4 also modestly contributes to *Y. pseudotuberculosis*–induced PP barrier dysfunction.

PP barrier dysfunction requires immune cells expressing TLR-2. A PP consists of aggregated immune cells organized in lymphoid follicles, overlaid by the specialized follicle-associated epithelium (FAE) (4). To determine whether the barrier dysfunction phenotype is dependent on TLR-2 expression on epithelial cells or on immune cells, we generated chimeric mice with somatic and/or hematopoietic cells expressing or lacking TLR-2. At the basal level, paracellular permeability was comparable in all chimeric mouse groups (Figure 2A). After exposure to pIB102, paracellular permeability was increased only in mice exhibiting a WT hematopoietic lineage that expressed TLR-2. Conversely, no changes were observed after infection of mice with a TLR-2–deficient hematopoietic lineage. Thus, the TLR-2 genotype of the epithelial cells had no effect on the phenotype. Comparable results were obtained when studying the translocation of *E. coli* (Figure 2B). Taken together, these results suggested that modulation of the PP barrier by *Y. pseudotuberculosis* depends exclusively on TLR-2 expression by cells of hematopoietic origin.

IL-1β production depends on the presence of TLR-2 in monocyte-derived cells. Previous studies indicated that IL-1β is produced by macrophages or DCs in response to *Y. pseudotuberculosis* infection and that it can modulate intestinal permeability (9, 10). We hypothesized that IL-1β is implicated in the observed results. 2 hours after TLR-2 stimulation by Pam4CSK3, IL-1β secretion was increased in THP-1 cells (Supplemental Figure 2). At 5 days after i.g. inoculation by pIB102, we observed an induction of IL-1β secretion in PPs and spleens of WT mice (Figure 3, A and B), whereas no or little IL-1β secretion was found in infected *Tlr2*$^{-/-}$ and *Myd88*$^{-/-}$ mice. These results indicated that TLR-2 expression is necessary to trigger IL-1β synthesis. To determine whether increased IL-1β production depends on TLR-2 expression on epithelial cells or on immune cells, we monitored IL-1β synthesis in TLR-2 chimeric mice. After exposure to pIB102, the elevated level of IL-1β was observed only in PPs of mice exhibiting a WT hematopoietic lineage expressing TLR-2 (Figure 3C).

To study the production of IL-1β in a better-controlled system, we infected bone marrow–derived macrophages and DCs in vitro with pIB102. After 6 hours, IL-1β expression was induced in cells derived from WT mice, whereas only moderate changes were seen in cells from *Tlr2*$^{-/-}$ and *Myd88*$^{-/-}$ mice (Figure 3, D and E). Similarly, in THP-1 cells, we observed IL-1β induction after exposure to pIB102 that was abolished when TLR-2 was inhibited by RNA silencing (Figure 4A). Similarly, TNF-α production was weakly (albeit significantly) reduced in case of TLR-2 inhibition by RNA silencing (Supplemental Figure 3 and Supplemental Methods). In contrast, TLR-2 inhibition did not affect IL-8 or IL-12 synthesis (Supplemental Figure 3 and Supplemental Methods). Finally, given that TLR-4 agonists induced IL-1β synthesis in THP-1 cells (Supplemental Figure 2), we studied the effect of TLR-4 inhibition on the synthesis of IL-1β, IL-8, IL-12, and TNF-α in response to pIB102. TLR-4 depletion by RNA silencing reduced, but did not completely abrogate, IL-1β synthesis (Figure 4A). TLR-4 depletion by RNA silencing also reduced TNF-α synthesis by infected THP-1 cells, but did not alter IL-8 or IL-12 production (Supplemental Figure 3, A and B, and Supplemental Methods).

For IL-1β production, 2 distinct events are required: enhanced synthesis of the pro–IL-1β precursor, and pro–IL-1β processing, which depends on caspase-1 activation in macrophages and DCs. TLR-2 silencing in THP-1 cells abrogated both pro–IL-1β production and caspase-1 activity (Figure 4, B and C). In addition, *Yersinia* infection increased *Tlr2* mRNA level while it decreased *Tlr4* mRNA level (Figure 4, D and E). Inhibition of caspase-1 activity by the selective inhibitor Z-YVAD-FMK suppressed pIB102-induced synthesis of IL-1β by THP-1 cells, but did not alter secretion of IL-8, IL-12, or TNF-α (Supplemental Figure 4 and Supplemental Methods). We thus conclude that after *Y. pseudotuberculosis* infection, IL-1β production through caspase-1 activation depends on TLR-2 expression.

The virulence plasmid of Yersinia is required for Y. pseudotuberculosis–induced IL-1β production and for alteration of epithelial barrier function in PPs. *Yersinia* species harbor a virulence plasmid encoding a type III secretion system that delivers bacterial proteins into the cytosol of targeted host cells. The translocator proteins YopB, YopD, and LcrV form a pore in host cell membranes that allow for translocation of 7 effector Yops into the cytosol (28). The role of the virulence plasmid on IL-1β synthesis and disruption of PP barrier function was

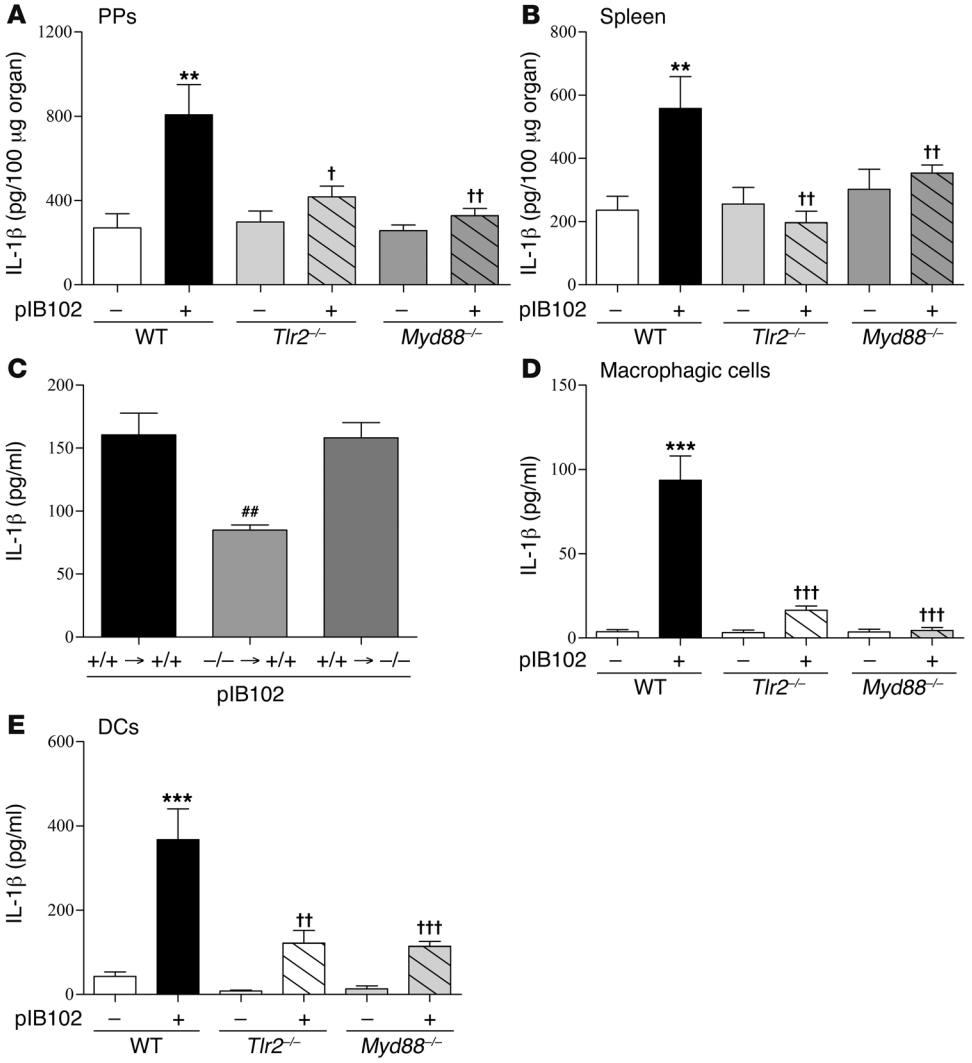

Figure 3
Increased IL-1β expression triggered by *Y. pseudotuberculosis* is mediated by TLR-2. (**A** and **B**) WT, *Tlr2*$^{-/-}$, and *Myd88*$^{-/-}$ mice were inoculated i.g. with pIB102 and killed 5 days after infection. PPs (**A**) and spleens (**B**) were removed, and IL-1β levels were analyzed. (**C**) PPs from chimeric mice were incubated with pIB102 in UCs. (**D** and **E**) BMSCs from WT, *Tlr2*$^{-/-}$, and *Myd88*$^{-/-}$ mice were differentiated into macrophages (**D**) or DCs (**E**) and infected with pIB102. IL-1β level in the supernatant was then analyzed by ELISA. $n \geq 6$ per group; 3 independent experiments. $^{**}P < 0.01$, $^{***}P < 0.001$ versus uninfected WT; $^{\dagger}P < 0.05$, $^{\dagger\dagger}P < 0.01$, $^{\dagger\dagger\dagger}P < 0.001$ versus pIB102-infected WT; $^{\#\#}P < 0.01$ versus pIB102-infected +/+ → +/+.

studied using genetically modified derivates of the WT *Y. pseudotuberculosis* strain. *Y. pseudotuberculosis* strain YPIII(pIB604) (referred to herein as pIB604) does not express YopB and may not form the pore necessary for translocation of the effector Yops.

Compared with pIB102, pIB604 induced a weaker (albeit significant) increase of IL-1β production and caspase-1 activation in vitro (Figure 5, A–E). Consistently, IL-1β levels measured in the supernatant of PPs infected ex vivo were increased with pIB102, but not with pIB604 (Figure 5F). Finally, paracellular and transcellular permeabilities remained low in PPs that were mounted in UCs and exposed to pIB604 (Figure 5, G and H). Together, these results suggested that the virulence plasmid of *Yersinia* is essential for *Y. pseudotuberculosis*–induced IL-1β production and increased permeability in PPs.

IL-1β contributes to the induction of barrier dysfunction in PPs. To investigate whether the increased production of IL-1β participates in PP barrier dysfunction, we treated WT mice with either Z-YVAD-FMK or the IL-1R antagonist anakinra, then assessed PP permeability in UCs. In the absence of *Y. pseudotuberculosis*, the fluxes of FD4 and *E. coli* through PPs were comparable in untreated and Z-YVAD-FMK– or anakinra-treated mice. In contrast, after exposure to pIB102, both Z-YVAD-FMK and anakinra abolished the increase of FD4 flux and *E. coli* translocation through PPs (Figure 6, A and B). To further validate the role of IL-1β, we repeated the experiments in mice deficient for the IL-1 receptor (*Il1r*$^{-/-}$ mice). In this model, no increase in paracellular flux of FD4 or *E. coli* translocation was observed in PPs exposed to pIB102 (Figure 6, A and B). Together, these results indicated that after *Y. pseudotuberculosis* infection, increased permeability requires caspase-1 activation and IL-1R expression.

Y. pseudotuberculosis–infected THP-1 cells stimulate paracellular and transcellular permeabilities in Caco-2 cells via IL-1β release and NF-κB activation. To better explore the crosstalk between immune and epithelial cells, we cocultured THP-1 cells with Caco-2 cells. Before coculture, THP-1 cells were infected or not with pIB102 and treated with gentamycin to kill the bacteria. Antibiotic-treated cells were then added to the basolateral compartment of Transwell chambers (TCs) harboring a polarized Caco-2 monolayer expressing the IL-1β receptor (Supplemental Table 2). After 24 hours of coculture, FD4 flux and *E. coli* translocation were significantly higher in infected THP-1 cells (Figure 7, A and B). Because adding the supernatant of infected THP-1 cells to the TC basolateral compartment recapitulated this phenomenon (Figure 7A), we concluded that it is mediated by a soluble factor secreted by the infected THP-1 cells.

To test the role of IL-1β, we added anakinra into the basolateral compartment of the TCs 24 hours before adding infected THP-1

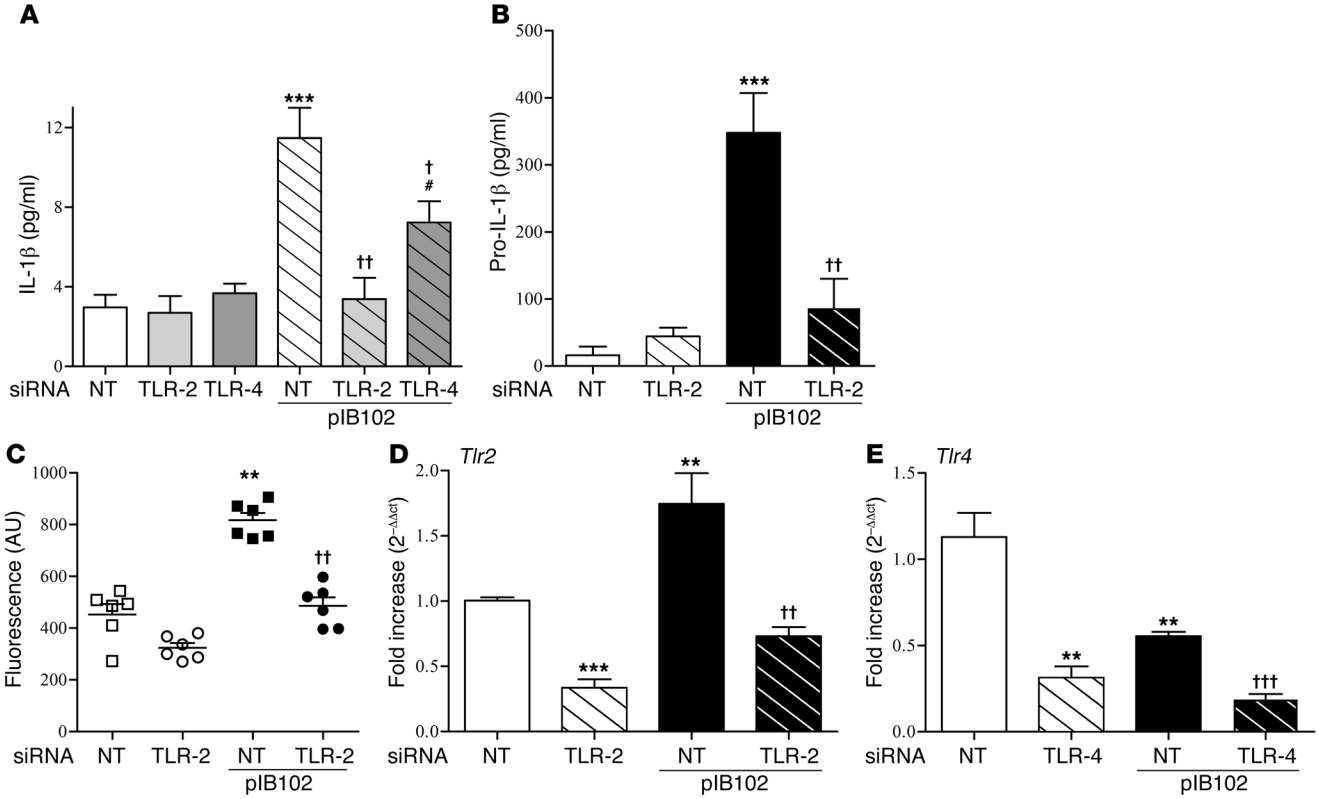

Figure 4

TLR2 and TLR4 are required for the *Y. pseudotuberculosis*–induced increase in IL-1β secretion in THP-1 cells. (**A**–**D**) THP-1 cells were transfected with TLR-2 or TLR-4 siRNA or with nontargeted (NT) control siRNA and infected with pIB102. After centrifugation, levels of IL-1β were measured in the supernatant (**A**), and levels of pro–IL-1β (**B**), caspase-1 activity (**C**), *Tlr2* mRNA (**D**), and *Tlr4* mRNA (**E**) were measured in the cell pellets. $n \geq 6$ per group; 3 independent experiments. $^{**}P < 0.01$, $^{***}P < 0.001$ versus uninfected NT; $^{\dagger}P < 0.05$, $^{\dagger\dagger}P < 0.01$, $^{\dagger\dagger\dagger}P < 0.001$ versus pIB102-infected NT; $^{\#}P < 0.05$ versus uninfected TLR-4.

cells. This procedure prevented the increase in FD4 flux and in *E. coli* translocation (Figure 7, A and B), which confirmed the role of the IL-1β receptor. Because infected THP-1 cells also produced TNF-α (Supplemental Figure 3C), which is also known to increase gut permeability (29), we also tested the effect of the anti–TNF-α antibody infliximab (Remicade; 25, 50, and 100 μg/ml) added into the basolateral compartment of the TCs. This procedure did not prevent the increase in FD4 flux (Supplemental Figure 3D), which confirmed the specific role of IL-1β in the alterations of Caco-2 barrier function in response to infected THP-1 cells.

To better understand the mechanisms involved in barrier dysfunction, we next investigated TJs by electron microscopy and immunostaining. To examine the TJ structure, we measured TJ width, a parameter that has previously been proposed to reflect the TJ intercellular space (30, 31). The functional alterations of the polarized Caco-2 monolayer were associated with increased TJ width (Figure 7, C and D) and redistribution of occludin (Figure 7E). In addition, Western blot analyses showed reduced occludin levels in Caco-2 cells cocultivated with infected THP-1 cells (Figure 7F). In contrast, zonula occludens–1 (ZO-1) localization was not affected (Figure 7E).

Finally, because previous studies have shown that IL-1β modifies paracellular permeability in Caco-2 cells via the NF-κB pathway (9), we also pretreated the Caco-2 cells with the NF-κB inhibitors ammonium pyrrolidine dithiocarbamate (PDTC) and caffeic acid phenethyl ester (CAPE). Consistent with the hypothesis of an IL-1β–driven mechanism, we observed reduced FD4 flux and *E. coli* translocation in pretreated cells (Figure 8, A and B). Similarly, treatment of PPs with PDTC, CAPE, or NBD peptide/NF-κB blockers reduced FD4 flux as well as *E. coli* translocation after pIB102 exposure (Figure 8, C and D).

Changes in epithelial cell functions depend on MLCK. Because previous studies described a central role of MLCK in controlling intestinal permeability, and because NF-κB activity might regulate MLCK expression in response to IL-1β stimulation (9), we studied the role of MLCK. After pIB102 infection, increased *MLCK* mRNA levels were observed in PPs from WT mice, but not from *Il1r*$^{-/-}$ or *Tlr2*$^{-/-}$ mice (Figure 9A). Furthermore, the increase of *MLCK* mRNA expression was observed only in chimeric mice of WT hematopoietic lineage expressing TLR-2 (Figure 9B). These in vivo observations indicated that transcription of *MLCK* mRNA is driven by IL-1β receptor expression by epithelial cells and TLR-2 expression by immune cells. In accordance with this observation, MLCK expression was significantly upregulated in Caco-2 cells cocultured with infected THP-1 cells (Figure 9C). This increased MLCK expression was abolished when Caco-2 cells were pretreated with an NF-κB inhibitor or with anakinra (Figure 9C). Finally, consistent with Caco-2 cells mainly expressing the long MLCK isoform, ELISA methods confirmed that MLCK protein levels paralleled those of mRNA (Figure 9D).

To further validate the role of MLCK, we pretreated WT mice with 3 MLCK inhibitors. After blockade of MLCK activity by i.p. adminis-

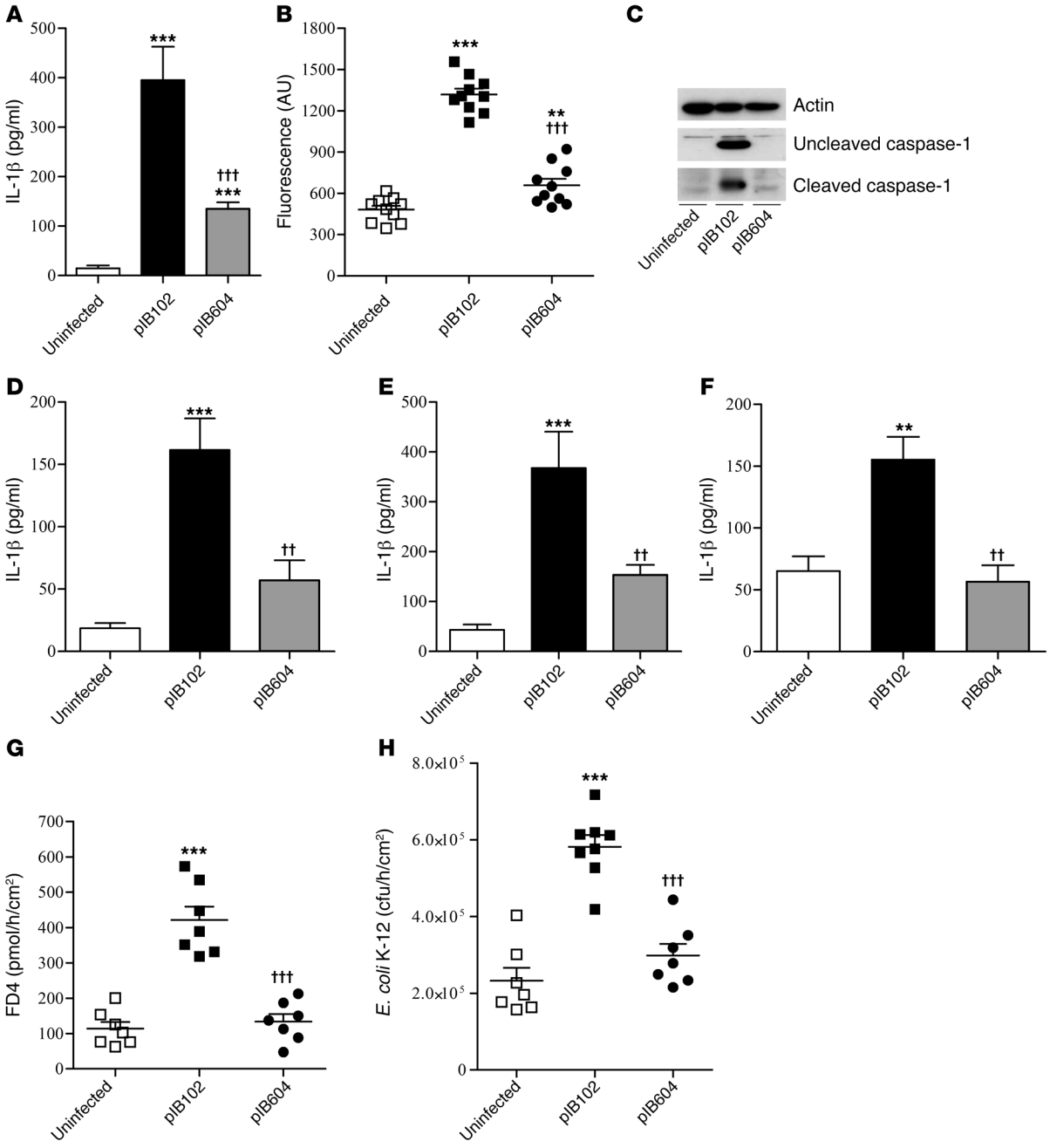

Figure 5

The virulence plasmid of *Yersinia* is required for *Y. pseudotuberculosis*–induced IL-1β increase and altered PP permeability. (**A**–**C**) THP-1 cells were infected with pIB102 or pIB604. After centrifugation, levels of IL-1β were measured in the supernatant (**A**), and caspase-1 activity was measured in the cell pellets (**B**). $n \geq 6$ per group; 3 independent experiments. (**C**) Western blot analyses of the uncleaved and cleaved caspase-1 (20-kDa) forms. (**D** and **E**) Bone morrow precursors from WT mice were differentiated into macrophages (**D**) or DCs (**E**) and infected with pIB102 or pIB604. IL-1β level in the supernatant was analyzed by ELISA. $n = 6$ per group; 3 independent experiments. (**F**) PPs were removed from WT mice and incubated with pIB102 or pIB604. After 6 hours, levels of IL-1β in the supernatant were determined by ELISA. $n \geq 6$ per group; 3 independent experiments. (**G** and **H**) PPs from WT mice were mounted in UCs and incubated with pIB102 or pIB604, and (**G**) paracellular permeability and (**H**) fluorescent *E. coli* K-12 translocation were monitored. $n = 8$ per group; 3 independent experiments. $^{**}P < 0.01$, $^{***}P < 0.001$ versus uninfected; $^{††}P < 0.01$, $^{†††}P < 0.001$ versus pIB102.

tration of inhibitors ML-7, ML-9, or peptide 18, no changes in feces excretion or food intake were observed. FD4 flux and *E. coli* translocation were no longer increased in PPs infected by pIB102 (Figure 10, A and B). Similarly, in TCs, pretreatment of Caco-2 cells with ML-7 or ML-9 abolished the increase of paracellular permeability and *E. coli* translocation triggered by infected THP-1 cells (Figure 10, C and D). Furthermore, in Caco-2 monolayers, phosphorylation of MLC by MLCK was increased in infected THP-1 cells (Figure 10E). Finally, a

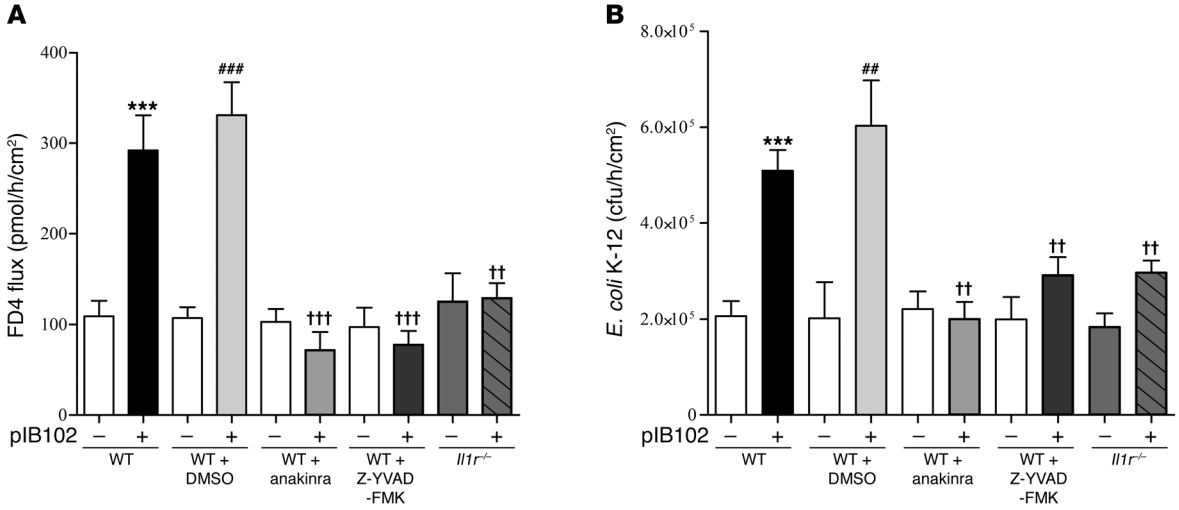

Figure 6
IL-1β expression induced by *Y. pseudotuberculosis* alters PP barrier function. (**A** and **B**) PPs from WT and *Il1r*$^{-/-}$ mice were mounted in UCs and incubated with pIB102, and (**A**) paracellular permeability and (**B**) fluorescent *E. coli* K-12 translocation were monitored. Where indicated, WT mice were treated i.p. with anakinra (300 μg/mouse) or Z-YVAD-FMK (100 μg/mouse) 2 days before experimentation. During experimentation, anakinra (50 μg/ml) or Z-YVAD-FMK (20 μg/ml) was added inside UCs. n = 8 per group; 3 independent experiments. ***P < 0.001 versus uninfected WT; ††P < 0.01, †††P < 0.001 versus pIB102-infected WT; ##P < 0.01, ###P < 0.001 versus uninfected WT plus DMSO.

higher density of actomyosin cytoskeleton adjacent to the TJ complexes was seen in Caco-2 monolayers cocultivated with infected THP-1 cells (Supplemental Figure 5). All these findings further demonstrated the crucial role of MCLK activation.

Discussion

Previously reported in vitro data have shown that *Y. pseudotuberculosis* affects gut permeability via paracellular and transcellular routes (26, 32). In addition, an increase of paracellular permeability is observed in patients with a history of *Y. pseudotuberculosis* infection compared with healthy controls (24, 25). Here, we confirmed by in vitro and in vivo experiments in mice that *Y. pseudotuberculosis* altered both paracellular and transcellular routes across the FAE of PPs. Moreover, we propose a comprehensive mechanism by which *Y. pseudotuberculosis* disrupts PP homeostasis (Supplemental Figure 6): hematopoietic immune cells infected by *Y. pseudotuberculosis* secrete IL-1β through TLR-2 activation. In response to IL-1β, NF-κB is activated in IECs of the FAE, which in turn activates MLCK and alters TJ structure.

Interestingly, other pathogenic bacteria, such as *L. monocytogenes*, *S. typhimurium*, *Clostridium difficile*, and some *E. coli* may also alter epithelial barrier function (33–37). However, the involved mechanisms differ from those described herein for *Y. pseudotuberculosis*. *S. typhimurium* and *C. difficile* toxin A increase paracellular permeability in colonic epithelial T84 cells via mechanisms involving the GTPases of the Rho family and protein kinase C (36, 38). *L. monocytogenes* increases paracellular permeability through a mechanism involving calcium influx (33, 34, 39). The adherent-invasive *E. coli* LF82 strain induces claudin-2 expression and a barrier defect in mice (37). Finally, enteropathogenic *E. coli* alters the epithelial TJ barrier through intracellular Ca^{2+} changes and MLCK phosphorylation (39). Thus, the mechanism described herein appears to be specific to *Y. pseudotuberculosis*.

The host response to *Y. pseudotuberculosis* involves TLR-2, which triggers recruitment and activation of intracellular kinases and, subsequently, expression of specific genes involved in host defense. In humans, TLR-2 mutations have been linked to increased susceptibility to infectious diseases (40, 41). Our data support the key role of TLR-2 after *Y. pseudotuberculosis* infection by demonstrating its role in intestinal barrier dysfunction. This finding is consistent with recent reports showing that TLR-2 activation is involved in transepithelial transport of microparticles (16, 32) and transcellular permeability through PPs (42). However, the effect of TLR-2 activation on gut permeability is still subject to debate, and some studies argue for a protective role of TLR-2 on intestinal permeability. In vitro, TLR-2 induces a modest reinforcement of epithelial barrier function by enhancing attachment of ZO-1 at the TJs in Caco-2 cells (43). TLR-2 stimulation has also been shown to reduce intestinal inflammation by transitorily improving epithelial barrier capacity in mice (44). In contrast, TLR-2 stimulation activates the immune system, enhancing the synthesis of inflammatory cytokines like TNF-α, IL-1β, or IL-8 and participating in colitis development in mice (45–47).

To date, most available data analyzing intestinal permeability were derived from in vitro experiments exploring isolated cell types. However, the in vivo effect of TLR-2 on PP permeability likely results from an interaction among several cell types, as suggested by the proximity and functional organization of epithelial cells, macrophages, DCs, and lymphocytes within PPs. To better account for this complexity, we developed in vitro and in vivo models, which allow for the exploration of cell interactions, such as cocultures of infected monocytes and epithelial cell or hematopoietic chimeric mice. We were thus able to demonstrate that the TLR-2–dependent increase in permeability was carried by immune cells from PPs.

With respect to the mechanisms linking TLR-2 activation in immune cells and the increased permeability from the Caco-2 monolayer, it appeared that the increased permeability was mediated by IL-1β. Recent studies using Caco-2 cells indicate that IL-1β increases paracellular permeability via increased MLCK expression and activity (9, 10). Consistently, we observed that IL-1β increased MLCK levels and activity within the epithelial cells of the FAE.

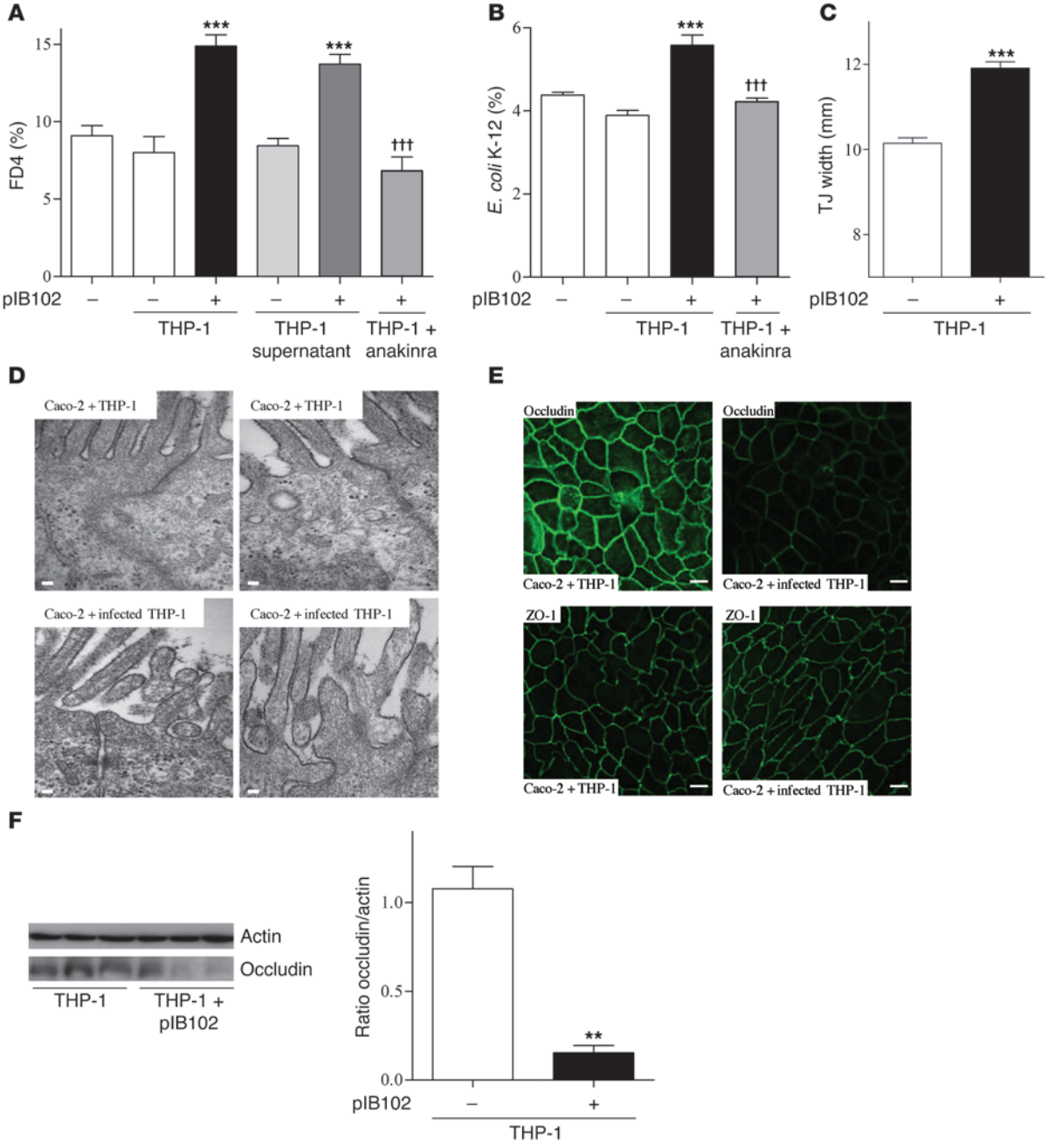

Figure 7

IL-1β secreted by *Y. pseudotuberculosis*–infected THP-1 cells alters paracellular permeability and *E. coli* translocation across Caco-2 monolayers. (**A**) Caco-2 and (**B**) Caco-2 clone-1 cells were cultivated into TCs. Then, THP-1 cells infected or not with pIB102 were added to the TC basolateral compartment, and (**A**) paracellular permeability and (**B**) *E. coli* translocation were monitored. To investigate the involvement of IL-1β receptor, Caco-2 and Caco-2 clone-1 cells were treated for 24 hours with anakinra (50 μg/ml). $n \geq 10$ per group; 3 independent experiments. ***$P < 0.001$ versus basal (–); †††$P < 0.001$ versus pIB102-infected THP-1. (**C** and **D**) TJ width of Caco-2 cells incubated with infected THP-1 cells was measured by EM. Scale bars: 100 nm. $n = 150$ measures of TJs per group from 3 independent wells. ***$P < 0.001$ versus uninfected THP-1. (**E**) Apical distribution of occludin and ZO-1 of Caco-2 cells incubated with infected THP-1 cells was analyzed by confocal microscopy. Scale bar: 20 μm. (**F**) Western blot analysis of occludin in Caco-2 cells incubated with infected THP-1 cells. $n = 3$ per group. **$P < 0.01$ versus uninfected THP-1.

MLCK plays a central role in the regulation of intestinal permeability (2, 48). For example, inhibition of MLCK prevents or reverses the opening of TJs induced by Na^+ nutrient cotransports (49), bacterial and parasitic infections (39, 50, 51), or inflammatory cytokines (7–9). Activation of MLCK catalyzes phosphorylation of MLC, which in turn induces contraction of perijunctional actin-myosin filaments and reorganization of the F-actin filament, occludin, and ZO-1, producing an opening of the TJ barrier (2). In agreement with these studies, our present results showed that MLCK activation induced by *Y. pseudotuberculosis* modified TJ architecture, as demonstrated by

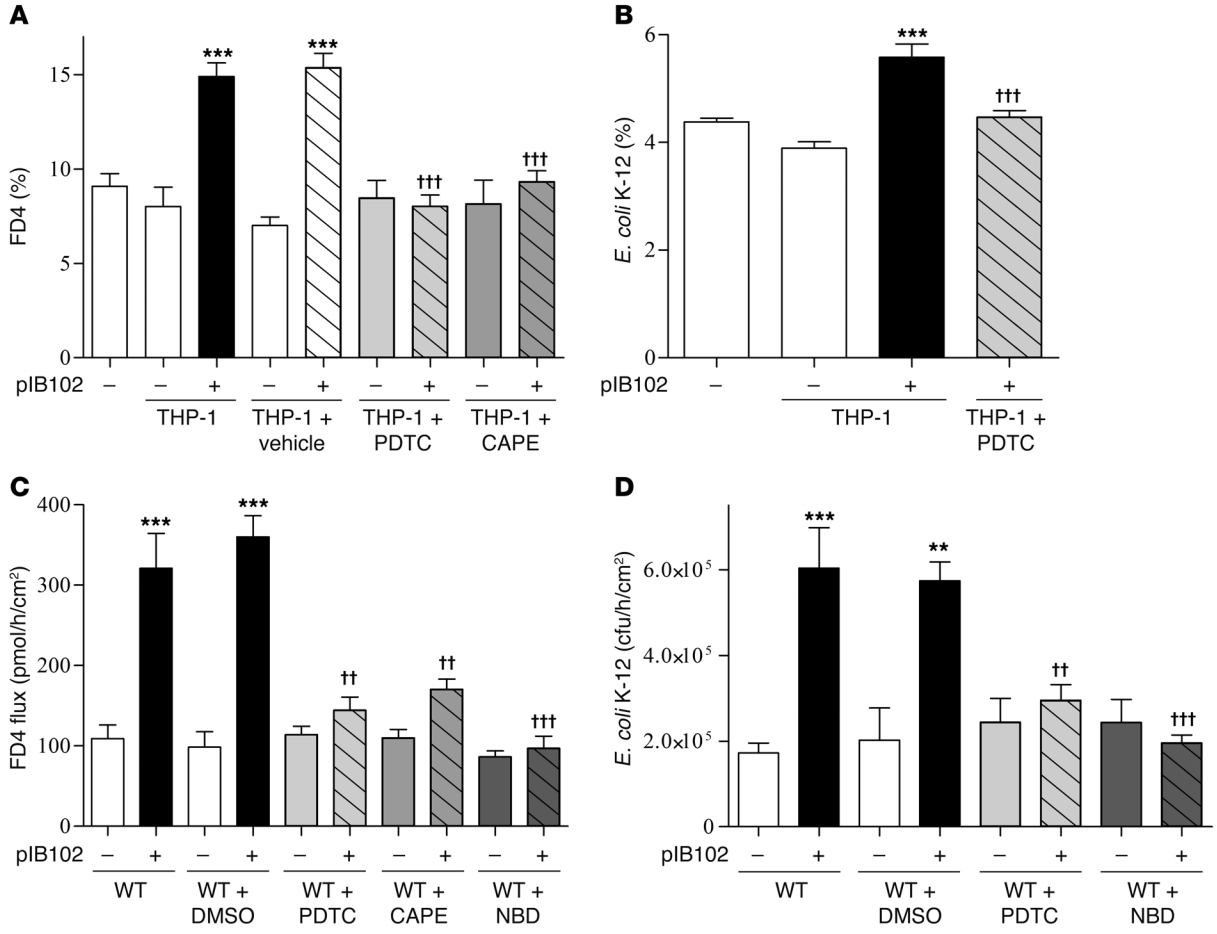

Figure 8

IL-1β released by THP-1 cells in response to *Y. pseudotuberculosis* alters paracellular and transcellular routes by increasing NF-κB activity in Caco-2 cells. (**A**) Caco-2 and (**B**) Caco-2 clone-1 cells were cultivated into TCs. Infected THP-1 cells were then added into the basolateral compartment of TCs, and (**A**) paracellular permeability and (**B**) *E. coli* translocation were monitored. To investigate the involvement of NF-κB in the increase of paracellular and *E. coli* translocation, cells were treated for 24 hours with PDTC (30 μg/ml) or CAPE (20 μg/ml). $n = 10$ per group; 3 independent experiments. ***$P < 0.001$ versus basal (–); †††$P < 0.001$ versus pIB102-infected THP-1. (**C** and **D**) WT mice were treated i.p. with PDTC (50 μg/mouse), CAPE (50 mg/kg/d), or NBD peptide/NF-κB blocker (400 μg/mouse) for 2 consecutive days before experimentation. PPs from treated WT mice were then mounted in UCs and incubated with pIB102, and (**C**) paracellular permeability and (**D**) bacterial translocation of *E. coli* K-12 were monitored. $n \geq 8$ per group; 3 independent experiments. **$P < 0.01$, ***$P < 0.001$ versus uninfected WT; ††$P < 0.01$, †††$P < 0.001$ versus pIB102-infected WT plus DMSO.

increased TJ width and delocalization as well as by reduced occludin protein expression. Our findings lent further support to the concept that MLCK is a key enzyme for the regulation of paracellular permeability, and also provided a molecular explanation for the previously reported perturbations in apical structure of actin filaments and redistribution of occludin after *Y. pseudotuberculosis* infection (26).

Besides its effect on paracellular permeability, MLCK inhibition also prevents increased transcellular permeability across the FAE of PPs (27). This finding is consistent with previous studies showing that MLCK modulates the transcellular passage of antigens and microbes through PPs and that endocytosis events are increased after *Y. pseudotuberculosis* infection (32). Interestingly, one of the characteristic features of endocytosis is its dependence on actin cytoskeleton reorganization (52, 53). Because MLCK is able to reorganize the perijunctional F-actin network by phosphorylating MLC (2), its role in endocytosis regulation is plausible; further elucidation will require additional study.

In summary, we concluded that TLR-2/IL-1β signaling in immune cells, as well as the IL-1R/NF-κB/MLCK signaling cascade in epithelial cells, contributes to the PP dysfunctions that characterize intestinal infection by *Y. pseudotuberculosis*. Furthermore, *Y. pseudotuberculosis* alters both paracellular and transcellular PP permeability by enhancing the same molecular pathways. These data provide insight into the interaction between epithelial cells and immune cells in PPs during infection with enteropathogens.

Methods

Animals

All animals were on the C57BL/6 background. WT, *Il1r*$^{-/-}$ (54), *Tlr2*$^{-/-}$ (14), *Tlr4*$^{-/-}$, and *Myd88*$^{-/-}$ (55) mice were housed in an animal facility with free access to food (UAR pellets) and water. *Tlr2*$^{-/-}$ and *Myd88*$^{-/-}$ mice were provided by L. Dubuquoy (Université Lille Nord de France, Lille, France) and J.-C. Sirard (Institut Pasteur de Lille, Lille, France),

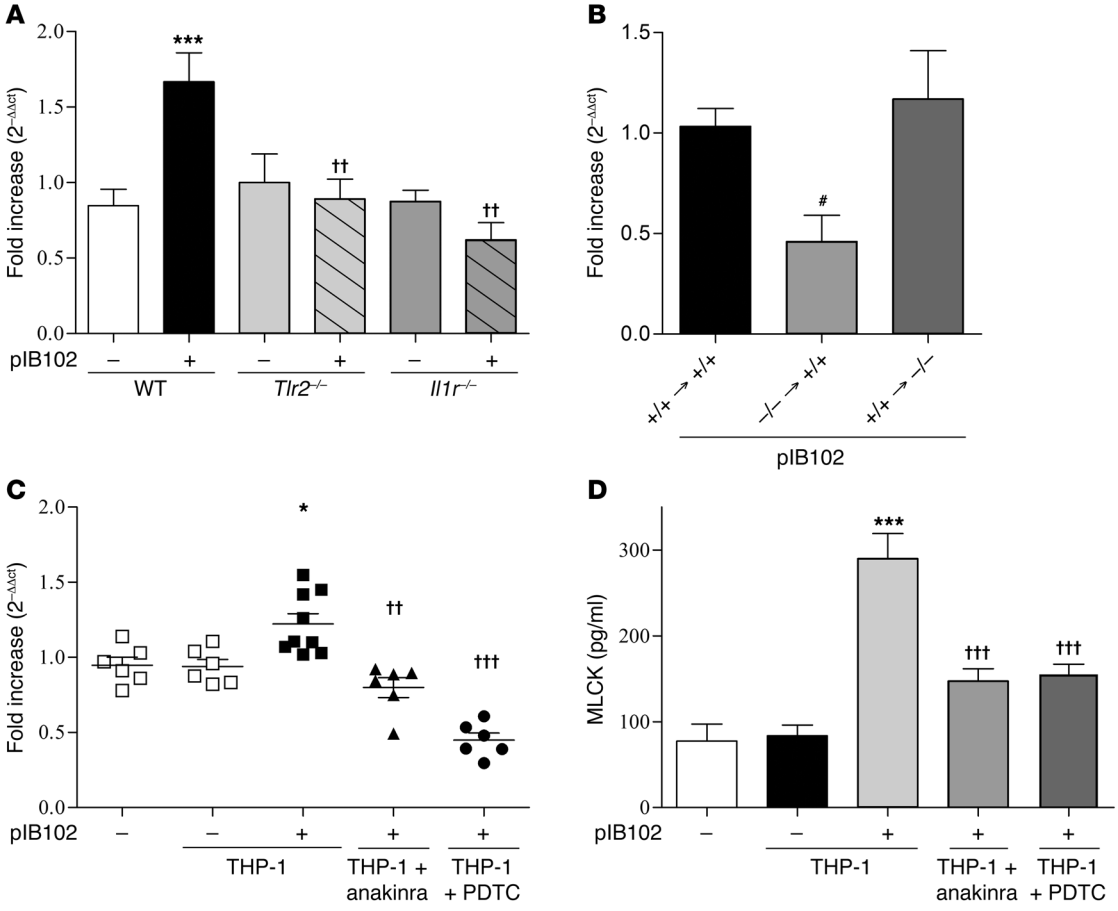

Figure 9

Y. pseudotuberculosis increases MLCK expression. (**A**) WT, *Il1r*$^{-/-}$, and *Tlr2*$^{-/-}$ mice were inoculated i.g. with pIB102, then killed 5 days after infection. PPs were removed, and mRNA expression of *MLCK* was determined by real-time PCR. n = 8 per group; 3 independent experiments. ***P < 0.001 versus uninfected WT; ††P < 0.01 versus pIB102-infected WT. (**B**) PPs from chimeric mice were removed and incubated for 6 hours with pIB102 in UCs, after which mRNA expression of *MLCK* was determined by real-time PCR. n = 6 per group; 2 independent experiments. #P < 0.05 versus pIB102-infected +/+ → +/+. (**C** and **D**) Caco-2 cells were cultivated into TCs, infected THP-1 cells were added into the TC basolateral compartment, and (**B**) mRNA expression and (**C**) protein level of MLCK were investigated after 24 hours of incubation. $n \geq 8$ per group; 3 independent experiments. *P < 0.05, ***P < 0.001 versus uninfected THP-1; ††P < 0.01, †††P < 0.001 versus pIB102-infected THP-1.

respectively. *Il1r*$^{-/-}$ and *Tlr4*$^{-/-}$ mice were provided by B. Ryffel (Université d'Orleans, Orleans, France). Pathogen-free conditions were maintained according to FELASA recommendations.

Bacterial strains and growth conditions

The *Y. pseudotuberculosis* strains studied were the YadA-deficient, invasin-positive strains YPIII(pIB102) and YPIII(pIB604) (56). Bacterial colonies harvested from fresh selective agar plates (kanamycin, 50 μg/ml) were grown overnight in Luria Broth medium (Sigma-Aldrich) containing kanamycin at 26°C, then for 2 hours at 37°C to induce the expression of virulence factors.

Cell lines

The Caco-2 cell line was purchased from the DSMZ collection. Caco-2 clone 1 was provided by A. Darfeuille-Michaud (Université de Clermont-Ferrand, Clermont-Ferrand, France). Caco-2 cells were grown at 37°C in a 5% CO_2 water-saturated atmosphere in Glutamax DMEM (Gibco, Invitrogen) supplemented with 20% heat-inactivated fetal bovin serum (Biowest), 1% nonessential amino acids and 1% antibiotics (100 U/ml penicillin and 100 mg/ml streptomycin; Gibco, Invitrogen). Cells were seeded in Transwell inserts (Costar) and grown for 14 days. THP-1 cells (obtained from ATCC) were grown at 37°C in a 5% CO_2 water-saturated atmosphere in RPMI-1640 (Gibco, Invitrogen) containing 10% heat-inactivated fetal bovine serum and 1% L-glutamine (Gibco, Invitrogen) supplemented with 1% antibiotics and 0.01% β-mercaptoethanol (Sigma-Aldrich).

Bone marrow–derived DCs and macrophages

DCs were derived from bone marrow stem cells (BMSCs) by culture in 2% conditioned medium from the GM-CSF–producing J558 hybridoma, as previously described (57). They were used at day 10. To obtain macrophagic cells, BMSCs were cultured for 6 days in medium supplemented with M-CSF containing supernatants from the L929 cell line (58).

Y. pseudotuberculosis infection

Animal infection. Mice were i.g. inoculated with a single dose of *Y. pseudotuberculosis* (10^7 cfu in 100 μl sterile water). At day 5, gut permeabilities and IL-1β concentrations were assessed in PPs and spleens.

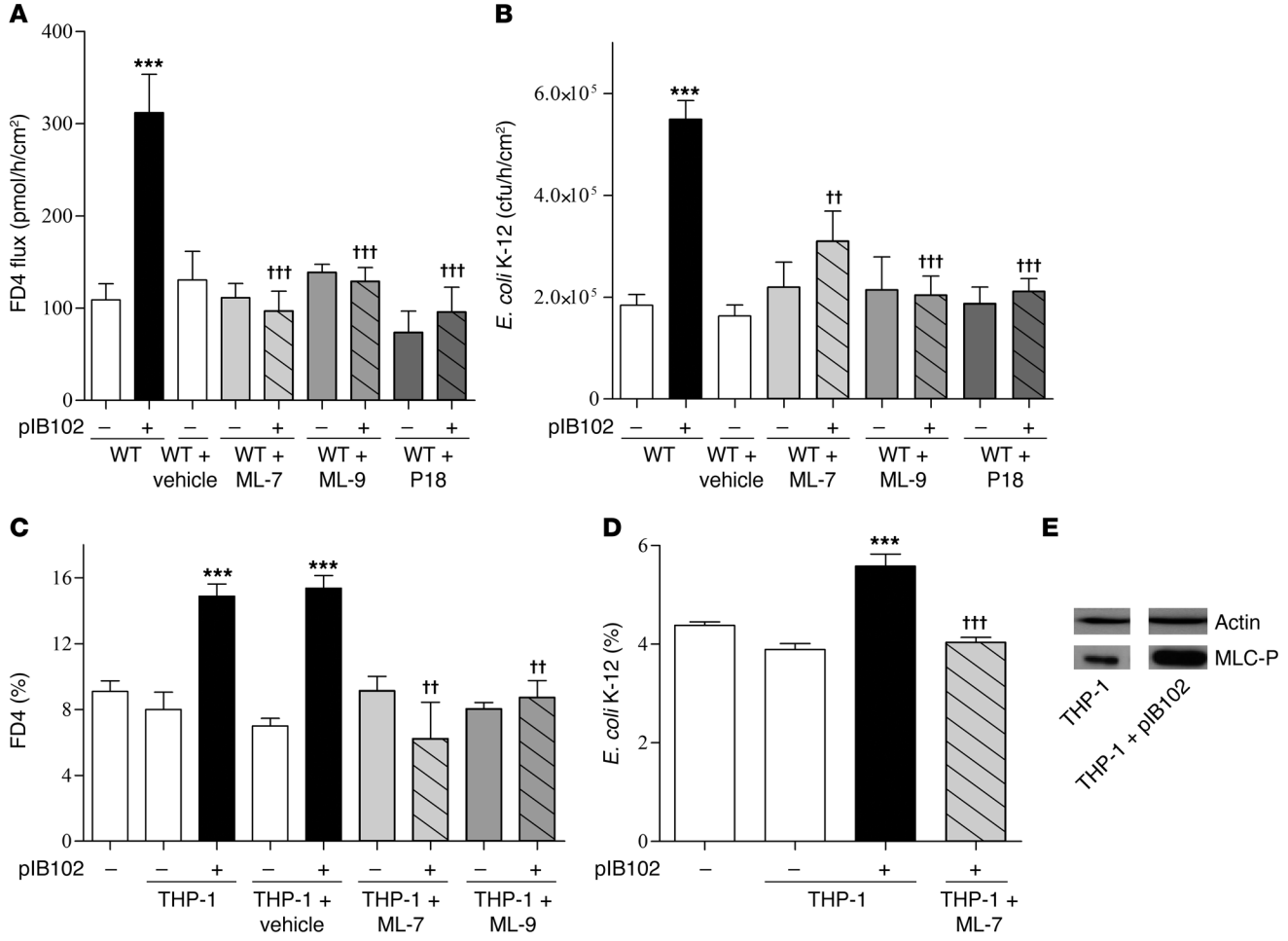

Figure 10

Y. pseudotuberculosis disrupts epithelial barrier functions by modulating MLCK activity. (**A** and **B**) WT mice were treated i.p. with ML-7 (2 mg/kg), ML-9 (2 mg/kg), or peptide 18 (P18; 100 μg/mouse) for 2 consecutive days before experimentation. PPs from treated WT mice were then mounted in UCs and incubated with pIB102, and (**A**) paracellular permeability and (**B**) bacterial translocation of *E. coli* K-12 were monitored. $n \geq 8$ per group; 3 independent experiments. ***$P < 0.001$ versus uninfected WT; ††$P < 0.01$, †††$P < 0.001$ versus pIB102-infected WT. (**C** and **D**) Caco-2 (**C**) and Caco-2 clone-1 (**D**) cells were cultivated into TCs. After 24 hours of ML-7 or ML-9 (50 μg/ml) treatment, infected THP-1 cells were added into the TC basolateral compartment, and (**C**) paracellular permeability and (**D**) *E. coli* translocation were monitored. $n \geq 8$ per group; 3 independent experiments. ***$P < 0.001$ versus uninfected THP-1; ††$P < 0.01$, †††$P < 0.001$ versus pIB102-infected THP-1. (**E**) MLCK activity was assessed by measuring phosphorylation of MLC (MLC-P) in Caco-2 cells by Western blot analyses. A representative blot of 3 independent experiments is shown.

Ex vivo infection of PPs. After mouse sacrifice, PPs were mounted in UCs, and pIB102 or pIB604 (1.5×10^7 cfu/ml) was added into the mucosal compartment. To test the effects of IL-1β, NF-κB, and MLCK, mice were pretreated i.p. with anakinra (300 μg/mouse/d), Z-YVAD-FMK (100 μg/mouse/d; Kamiya Biomedical), PDTC (50 μg/mouse/d; Calbiochem), CAPE (50 mg/kg/d; Sigma-Aldrich), NBD peptide/NF-κB blocker (400 μg/mouse/d; Enzo Life Sciences), ML-7 (2 mg/kg; Sigma-Aldrich), ML-9 (4 mg/kg; Sigma-Aldrich), or peptide 18 (100 μg/mouse/d; Merck) for 2 consecutive days before experimentation. When indicated, anakinra (50 μg/ml), Z-YVAD-FMK (20 μg/ml), PDTC (30 μg/ml), CAPE (20 μg/ml), NBD (20 μM), ML-7 (20 μg/ml), ML-9 (50 μg/ml), peptide 18 (250 μM), or the same amount of vehicle was used in the mucosal compartment of UCs.

Cell infection. DCs, macrophages, or THP-1 cells were infected by adding pIB102 or pIB604 (MOI 10). After 2 or 6 hours, extracellular bacteria were killed by adding gentamycin (100 μg/ml; Sigma-Aldrich), and IL-1β levels were measured by ELISA in the supernatants.

Permeability measurements

In vivo. Mice were gavaged with FD4 or FD40 (15 mg/100 μl/mouse; Sigma-Aldrich) 5 hours prior to sacrifice. Whole serum FD4 or FD40 levels were determined with a fluorometer (PerkinElmer).

Ex vivo. After mouse sacrifice, PPs were mounted in UCs and maintained in circulating oxygenated Ringer solution at 37°C throughout the experiment. Paracellular permeability was assessed 2 hours after infection by measuring the mucosal-to-serosal flux of FD4. Bacterial translocation was measured at 2 hours using chemically killed fluorescein-conjugated *E. coli* K-12 strain (Molecular Probes) added at a final concentration of 1×10^7 cfu/ml in the mucosal reservoir.

In vitro. Paracellular permeability was investigated using the Caco-2 cell line, whereas *E. coli* translocation was monitored on Caco-2 clone 1 (9, 32).

Coculture. FD4 (10^{-5} M) or *E. coli* K-12 strain (1×10^7 cfu/ml) were added into the apical compartment of the TC. Permeability was monitored by sampling 400 μl from the basolateral compartment 24 hours after addi-

tion of 1 × 10^6 THP-1 cells, infected or not with *Y. pseudotuberculosis*, in the basolateral chamber. When indicated, Caco-2 cells were preincubated for 24 hours with PDTC (30 μg/ml), CAPE (20 μg/ml), anakinra (50 μg/ml), ML-7 (20 μg/ml), or ML-9 (50 μg/ml).

Chimeric mice

BMSCs were isolated from WT Ly5.1 or *Tlr2*$^{-/-}$ Ly5.2 mice. 5 × 10^6 cells were injected i.v. into *Tlr2*$^{+/+}$ Ly5.1 or *Tlr2*$^{-/-}$ Ly.5.2 lethally irradiated recipients. Chimerism was assessed at week 12 by flow cytometry using the Ly5.1 and Ly5.2 markers (Supplemental Figure 7 and Supplemental Methods).

*IL-1*β

In vivo. 5 days after infection, PPs and spleens from WT, *Tlr2*$^{-/-}$, and *Myd88*$^{-/-}$ mice were removed, washed, and homogenized in PBS containing protease inhibitor (Roche). IL-1β levels were measured by ELISA (BD Biosciences).

Ex vivo. PPs from WT mice were removed and maintained in circulating oxygenated Ringer solution at 37°C. Then, PPs were infected with *Y. pseudotuberculosis* (1 × 10^7 cfu/ml). After 6 hours, IL-1β levels in the supernatant were measured.

In vitro. IL-1β concentrations in the supernatant were determined 6 hours after infection for BMSC-DCs and macrophages (MOI10) and 2 hours after infection for THP-1 cells (MOI10).

*Pro–IL-1*β

2 hours after infection, THP-1 cells were centrifuged and homogenized in PBS containing protease inhibitor. Pro–IL-1β concentrations were determined using a commercial ELISA kit (R&D systems).

Caspase-1 activity

2 hours after infection, THP-1 cells were centrifugated, and the pellets were incubated with the FLICA reagent (Immunochemistry Technologies). Pellets were washed, and the level of fluorescence — corresponding to caspase-1 activity — was determined using a fluorometer (PerkinElmer).

RT-PCR

After extraction by the NucleoSpin RNA II Kit (Macherey-Nagel), total RNA was converted to cDNA using random hexonucleotides. PCR was performed using QuantiTect SYBR Green PCR Kit (Applied) and sense and antisense primers specific for TLR-2, TLR-4, G3PDH, and the long isoform of MLCK. See Supplemental Table 1 for sequences. After amplification, we determined the Ct to obtain $2^{-\Delta\Delta Ct}$ expression values.

siRNAs

The ON-TARGET plus SMARTpool siRNAs targeting TLR-2 (L-005120-01-0005) and TLR-4 (L-008088-01) and the nontargeted (NT) control siRNA were purchased from Dharmacon. Transfections were done 48 hours before experiments. THP-1 cells were used according to the manufacturer's instructions (Invitrogen).

MLCK protein

Caco-2 cells were washed with PBS and lysed. MLCK concentrations (short and long isoforms) were determined by ELISA (Cusabio) according to the manufacturer's instructions.

Electron microscopy

Caco-2 filters were flushed with PBS, ligatured, and filled with glutaraldhehyde/tannic acid. Fine samples were cut and fixed by glutaraldhehyde/tannic acid. Samples were postfixed in osmic acid, then dehydrated in graded alcohol and embedded in Epon resin (Polysciences Inc). Ultrathin sections (65 nm) were counterstained with uranyl acetate and lead citrate using an LKB 2168 ultrostainer. Observations were made using a JEOL CX100 equipped with a Gatan Digital camera, and the micrographs were processed with Gatan software. Measurements of TJs were performed with NIH Image J software.

Immunohistochemistry

Caco-2 filters were washed in PBS and fixed with cold methanol. After incubation in PBS plus 1% BSA at room temperature, Caco-2 filters were incubated with anti-rabbit primary antibodies occludin (Zymed) and ZO-1 (Invitrogen), then washed in PBS. Filters were then incubated with Alexa Fluor 488 secondary antibody (Invitrogen). Fluoprep reagent solution (Biomerieux) was used to mount the filters on the coverslips.

Western blot analyses

Phosphorylated myosin light chain. Caco-2 monolayers were rinsed with PBS and scraped. Cell lysates were centrifuged, and supernatant was collected. Protein concentration was determined using a commercial kit. Proteins were boiled, separated on SDS-PAGE gel, and transferred to a membrane (iBlot gel transfer stacks, Nitrocellulose regular; Invitrogen). The membrane was incubated overnight in a blocking solution containing anti–phospho–myosin light chain (Ser19) (Cell Signaling). After washing, the membrane was incubated with HRP-conjugated antibody (GE Healthcare) and developed using Super Signal West Pico Chemiluminescent Substrate (Thermo Scientific) on the Amersham Hyperfilm film ECL.

Occludin. Caco-2 monolayers cultivated or not with infected THP-1 cells were processed as above. The membrane was incubated overnight with anti-occludin (Zymed).

Cleaved and noncleaved caspase-1. pIB102-infected THP-1 cells were processed as above. The membrane was incubated overnight with anti–cleaved caspase-1 (Temecula).

Statistics

Comparison of 2 groups was performed using unpaired *t* test (Mann-Whitney) with 2-tailed *P* value; comparison of multiple groups was performed using 1-way ANOVA. Statistical analyses were performed using GraphPad Prism 4.00 (GraphPad Software). A *P* value less than 0.05 was considered statistically significant (2-sided tests). Values are expressed as mean ± SEM.

Study approval

Housing and experiments were conducted according to institutional animal healthcare guidelines and were approved by the local ethical committee for animal experimentation (Comité Régional d'Ethique en matière d'Expérimentation Animale no. 4, Paris, France).

Acknowledgments

Financial support was provided by INSERM, the Université Paris-Diderot, and the Association François Aupetit.

Received for publication November 10, 2011, and accepted in revised form March 28, 2012.

Address correspondence to: Frédérick Barreau, INSERM U843, Hôpital Robert Debré, 48 Bd Sérurier, 75019 Paris, France. Phone: 33.1.57.27.73.27; Fax: 33.1.57.27.74.61; E-mail: frederick.barreau@inserm.fr.

1. Kagnoff MF, Eckmann L. Epithelial cells as sensors for microbial infection. *J Clin Invest*. 1997; 100(1):6–10.
2. Shen L, et al. Myosin light chain phosphorylation regulates barrier function by remodeling tight junction structure. *J Cell Sci*. 2006; 119(Pt 10):2095–2106.
3. Clayburgh DR, Shen L, Turner JR. A porous defense: the leaky epithelial barrier in intestinal

disease. *Lab Invest*. 2004;84(3):282–291.
4. Jung C, Hugot JP, Barreau F. Peyer's Patches: The immune sensors of the intestine. *Int J Inflam*. 2010; 2010:823710.
5. Su L, et al. Targeted epithelial tight junction dysfunction causes immune activation and contributes to development of experimental colitis. *Gastroenterology*. 2009;136(2):551–563.
6. Martin-Padura I, et al. Junctional adhesion molecule, a novel member of the immunoglobulin superfamily that distributes at intercellular junctions and modulates monocyte transmigration. *J Cell Biol*. 1998;142(1):117–127.
7. Clayburgh DR, et al. Epithelial myosin light chain kinase-dependent barrier dysfunction mediates T cell activation-induced diarrhea in vivo. *J Clin Invest*. 2005;115(10):2702–2715.
8. Wang F, Graham WV, Wang Y, Witkowski ED, Schwarz BT, Turner JR. Interferon-gamma and tumor necrosis factor-alpha synergize to induce intestinal epithelial barrier dysfunction by up-regulating myosin light chain kinase expression. *Am J Pathol*. 2005;166(2):409–419.
9. Al-Sadi R, Ye D, Dokladny K, Ma TY. Mechanism of IL-1beta-induced increase in intestinal epithelial tight junction permeability. *J Immunol*. 2008; 180(8):5653–5661.
10. Al-Sadi RM, Ma TY. IL-1beta causes an increase in intestinal epithelial tight junction permeability. *J Immunol*. 2007;178(7):4641–4649.
11. Cario E. Bacterial interactions with cells of the intestinal mucosa: Toll-like receptors and NOD2. *Gut*. 2005;54(8):1182–1193.
12. Hausmann M, et al. Toll-like receptors 2 and 4 are up-regulated during intestinal inflammation. *Gastroenterology*. 2002;122(7):1987–2000.
13. Lindsay JO, et al. Clinical, microbiological, and immunological effects of fructo-oligosaccharide in patients with Crohn's disease. *Gut*. 2006; 55(3):348–355.
14. Takeuchi O, et al. Differential roles of TLR2 and TLR4 in recognition of gram-negative and gram-positive bacterial cell wall components. *Immunity*. 1999;11(4):443–451.
15. Rakoff-Nahoum S, Paglino J, Eslami-Varzaneh F, Edberg S, Medzhitov R. Recognition of commensal microflora by toll-like receptors is required for intestinal homeostasis. *Cell*. 2004;118(2):229–241.
16. Chabot S, Wagner JS, Farrant S, Neutra MR. TLRs regulate the gatekeeping functions of the intestinal follicle-associated epithelium. *J Immunol*. 2006; 176(7):4275–4283.
17. Hamzaoui N, Kerneis S, Caliot E, Pringault E. Expression and distribution of beta1 integrins in in vitro-induced M cells: implications for Yersinia adhesion to Peyer's patch epithelium. *Cell Microbiol*. 2004;6(9):817–828.
18. Handley SA, Dube PH, Revell PA, Miller VL. Characterization of oral Yersinia enterocolitica infection in three different strains of inbred mice. *Infect Immun*. 2004;72(3):1645–1656.
19. Mecsas J, Bilis I, Falkow S. Identification of attenuated Yersinia pseudotuberculosis strains and characterization of an orogastric infection in BALB/c mice on day 5 postinfection by signature-tagged mutagenesis. *Infect Immun*. 2001;69(5):2779–2787.
20. Pepe JC, Wachtel MR, Wagar E, Miller VL. Pathogenesis of defined invasion mutants of Yersinia enterocolitica in a BALB/c mouse model of infection. *Infect Immun*. 1995;63(12):4837–4848.
21. Dessein R, et al. Toll-like receptor 2 is critical for induction of Reg3 beta expression and intestinal clearance of Yersinia pseudotuberculosis. *Gut*. 2009; 58(6):771–776.
22. Auerbuch V, Isberg RR. Growth of Yersinia pseudotuberculosis in mice occurs independently of Toll-like receptor 2 expression and induction of interleukin-10. *Infect Immun*. 2007;75(7):3561–3570.
23. Homewood R, Gibbons CP, Richards D, Lewis A, Duane PD, Griffiths AP. Ileitis due to Yersinia pseudotuberculosis in Crohn's disease. *J Infect*. 2003; 47(4):328–332.
24. Lahesmaa-Rantala R, Magnusson KE, Granfors K, Leino R, Sundqvist T, Toivanen A. Intestinal permeability in patients with yersinia triggered reactive arthritis. *Ann Rheum Dis*. 1991;50(2):91–94.
25. Serrander R, Magnusson KE, Kihlstrom E, Sundqvist T. Acute yersinia infections in man increase intestinal permeability for low-molecular weight polyethylene glycols (PEG 400). *Scand J Infect Dis*. 1986; 18(5):409–413.
26. Tafazoli F, Holmstrom A, Forsberg A, Magnusson KE. Apically exposed, tight junction-associated beta1-integrins allow binding and YopE-mediated perturbation of epithelial barriers by wild-type Yersinia bacteria. *Infect Immun*. 2000;68(9):5335–5343.
27. Barreau F, et al. Nod2 regulates the host response towards microflora by modulating T cell function and epithelial permeability in mouse Peyer's patches. *Gut*. 2010;59(2):207–217.
28. Viboud GI, Bliska JB. Yersinia outer proteins: role in modulation of host cell signaling responses and pathogenesis. *Annu Rev Microbiol*. 2005;59:69–89.
29. Ma TY, Boivin MA, Ye D, Pedram A, Said HM. Mechanism of TNF-{alpha} modulation of Caco-2 intestinal epithelial tight junction barrier: role of myosin light-chain kinase protein expression. *Am J Physiol Gastrointest Liver Physiol*. 2005;288(3):G422–G430.
30. Cattin AL, et al. Hepatocyte nuclear factor 4alpha, a key factor for homeostasis, cell architecture, and barrier function of the adult intestinal epithelium. *Mol Cell Biol*. 2009;29(23):6294–6308.
31. Nighot PK, Blikslager AT. ClC-2 regulates mucosal barrier function associated with structural changes to the villus and epithelial tight junction. *Am J Physiol Gastrointest Liver Physiol*. 2010; 299(2):G449–G456.
32. Ragnarsson EG, et al. Yersinia pseudotuberculosis induces transcytosis of nanoparticles across human intestinal villus epithelium via invasin-dependent macropinocytosis. *Lab Invest*. 2008; 88(11):1215–1226.
33. Tsuchiya K, Kawamura I, Takahashi A, Nomura T, Kohda C, Mitsuyama M. Listeriolysin O-induced membrane permeation mediates persistent interleukin-6 production in Caco-2 cells during Listeria monocytogenes infection in vitro. *Infect Immun*. 2005; 73(7):3869–3877.
34. Savkovic SD, Ramaswamy A, Koutsouris A, Hecht G. EPEC-activated ERK1/2 participate in inflammatory response but not tight junction barrier disruption. *Am J Physiol Gastrointest Liver Physiol*. 2001; 281(4):G890–G898.
35. Spitz J, Yuhan R, Koutsouris A, Blatt C, Alverdy J, Hecht G. Enteropathogenic Escherichia coli adherence to intestinal epithelial monolayers diminishes barrier function. *Am J Physiol*. 1995; 268(2 pt 1):G374–G379.
36. Hecht G, Pothoulakis C, LaMont JT, Madara JL. Clostridium difficile toxin A perturbs cytoskeletal structure and tight junction permeability of cultured human intestinal epithelial monolayers. *J Clin Invest*. 1988;82(5):1516–1524.
37. Denizot J, et al. Adherent-invasive Escherichia coli induce claudin-2 expression and barrier defect in CEABAC10 mice and crohn's disease patients. *Inflamm Bowel Dis*. 2012;18(2):294–304.
38. Chen ML, Pothoulakis C, LaMont JT. Protein kinase C signaling regulates ZO-1 translocation and increased paracellular flux of T84 colonocytes exposed to Clostridium difficile toxin A. *J Biol Chem*. 2002;277(6):4247–4254.
39. Yuhan R, Koutsouris A, Savkovic SD, Hecht G. Enteropathogenic Escherichia coli-induced myosin light chain phosphorylation alters intestinal epithelial permeability. *Gastroenterology*. 1997; 113(6):1873–1882.
40. Ogus AC, et al. The Arg753GLn polymorphism of the human toll-like receptor 2 gene in tuberculosis disease. *Eur Respir J*. 2004;23(2):219–223.
41. Schroder NW, Schumann RR. Single nucleotide polymorphisms of Toll-like receptors and susceptibility to infectious disease. *Lancet Infect Dis*. 2005; 5(3):156–164.
42. Barreau F, et al. Nod2 regulates the host response towards microflora by modulating T cell function and epithelial permeability in mouse Peyer's patches. *Gut*. 2010;59(2):207–217.
43. Cario E, Gerken G, Podolsky DK. Toll-like receptor 2 enhances ZO-1-associated intestinal epithelial barrier integrity via protein kinase C. *Gastroenterology*. 2004;127(1):224–238.
44. Cario E, Gerken G, Podolsky DK. Toll-like receptor 2 controls mucosal inflammation by regulating epithelial barrier function. *Gastroenterology*. 2007; 132(4):1359–1374.
45. Watanabe T, Kitani A, Murray PJ, Strober W. NOD2 is a negative regulator of Toll-like receptor 2-mediated T helper type 1 responses. *Nat Immunol*. 2004;5(8):800–808.
46. Watanabe T, et al. Muramyl dipeptide activation of nucleotide-binding oligomerization domain 2 protects mice from experimental colitis. *J Clin Invest*. 2008;118(2):545–559.
47. Hedl M, Li J, Cho JH, Abraham C. Chronic stimulation of Nod2 mediates tolerance to bacterial products. *Proc Natl Acad Sci U S A*. 2007; 104(49):19440–19445.
48. Ma TY, Tran D, Hoa N, Nguyen D, Merryfield M, Tarnawski A. Mechanism of extracellular calcium regulation of intestinal epithelial tight junction permeability: role of cytoskeletal involvement. *Microsc Res Tech*. 2000;51(2):156–168.
49. Turner JR, et al. Physiological regulation of epithelial tight junctions is associated with myosin light-chain phosphorylation. *Am J Physiol*. 1997; 273(4 pt 1):C1378–C1385.
50. Philpott DJ, McKay DM, Mak W, Perdue MH, Sherman PM. Signal transduction pathways involved in enterohemorrhagic Escherichia coli-induced alterations in T84 epithelial permeability. *Infect Immun*. 1998;66(4):1680–1687.
51. Scott KG, Meddings JB, Kirk DR, Lees-Miller SP, Buret AG. Intestinal infection with Giardia spp. reduces epithelial barrier function in a myosin light chain kinase-dependent fashion. *Gastroenterology*. 2002;123(4):1179–1190.
52. Swanson JA, Watts C. Macropinocytosis. *Trends Cell Biol*. 1995;5(11):424–428.
53. Amyere M, et al. Origin, originality, functions, subversions and molecular signalling of macropinocytosis. *Int J Med Microbiol*. 2002;291(6–7):487–494.
54. Labow M, et al. Absence of IL-1 signaling and reduced inflammatory response in IL-1 type I receptor-deficient mice. *J Immunol*. 1997;159(5):2452–2461.
55. Kawai T, Adachi O, Ogawa T, Takeda K, Akira S. Unresponsiveness of MyD88-deficient mice to endotoxin. *Immunity*. 1999;11(1):115–122.
56. Hakansson S, et al. The YopB protein of Yersinia pseudotuberculosis is essential for the translocation of Yop effector proteins across the target cell plasma membrane and displays a contact-dependent membrane disrupting activity. *EMBO J*. 1996;15(21):5812–5823.
57. Mederle I, et al. Plasmidic versus insertional cloning of heterologous genes in Mycobacterium bovis BCG: impact on in vivo antigen persistence and immune responses. *Infect Immun*. 2002;70(1):303–314.
58. Rousseau C, et al. Production of phthiocerol dimycocerosates protects Mycobacterium tuberculosis from the cidal activity of reactive nitrogen intermediates produced by macrophages and modulates the early immune response to infection. *Cell Microbiol*. 2004;6(3):277–287.